Received April 22, 2019, accepted May 8, 2019, date of publication May 15, 2019, date of current version May 28, 2019.

Digital Object Identifier 10.1109/ACCESS.2019.2917140

PKBPNN-Based Tracking Range Extending Approach for TMR Magnetic Tracking System

BOWEN LV[1,4], YUANGUI CHEN[2], HOUDE DAI[1], SHIJIAN SU[1,3], AND MINGQIANG LIN[1]

[1]Quanzhou Institute of Equipment Manufacturing, Haixi Institutes, Chinese Academy of Sciences, Jinjiang 362216, China
[2]Department of Radiation Oncology, Fujian Medical University Union Hospital, Fuzhou 350001, China
[3]School of Physics and Information Engineering, Fuzhou University, Fuzhou 350108, China
[4]School of Big Data, North University of China, Taiyuan 030000, China

Corresponding author: Houde Dai (dhd@fjirsm.ac.cn)

This work was supported in part by the Natural Science Foundation of China under Grant 61501428, in part by the Science and Technology Department of Fujian Province under 2018Y0036, and in part by the Quanzhou Science and Technology Plan Project under Grant 2017G014.

ABSTRACT The magnetic tracking system, which is based on a permanent magnet and a magnetometer array, has numerous potential applications in the biomedical and industrial area. However, its tracking accuracy drops off sharply with the increase of tracking distance because of both the interference of environmental magnetic field and sensor measurement noise. To extend the magnetic tracking range, two novel methods were proposed in this study. First, the state-of-the-art tri-axial tunnel magnetoresistance (TMR) sensors, which possess the most significant field sensitivity and signal-to-noise ratio (SNR) over other types of magnetoresistive sensors, were adopted to construct the sensor array. Second, a fusion approach was proposed for tracking range extending. The particle swarm optimization-Levenberg Marquardt (PSO-LM) method based on the magnetic dipole model was applied in the near field (*i.e.*, near-source zone), and the prior knowledge based back propagation neural network (PKBPNN) was adopted to the far field (*i.e.*, far-source zone). In the transition zone, these two algorithms were fused by using an adaptive sigmoid function. The trained artificial neural network (ANN) model embodied the physical model errors, the sensor installation errors, and the inherent characteristics of adopted magnetometers. Therefore, it has greater tracking performance than singly using the PSO-LM in the far-source zone. The experimental results show that the tracking errors decrease from (18.24 ± 9.37mm, $12.45 \pm 3.37°$) to (8.95 ± 1.74mm, $7.97 \pm 2.08°$) in the tracking range between 216 and 296 mm. Besides, the tracking distance is extended to 396 mm, with the position error of less than 25 mm. It can be concluded that this approach has significantly extended the tracking range of the magnetic tracking system.

INDEX TERMS Back propagation neural network (BPNN), magnetic tracking, prior knowledge, TMR, tracking range.

I. INTRODUCTION

A magnetometer array, which consists of several tri-axial magnetometers, is adopted as a sensing module in a magnetic tracking system, while a permanent magnet is functioned as the magnetic source [1]. By performing magnetic tracking algorithms based on the sensor data, the pose of the magnet in space can be calculated. This tracking approach, with sub-degree and sub-millimetric, has shown potential for both biomedical and industrial applications because of its advantages such as no line-of-sight problem, wireless, real-time, and low-cost [2], [3]. For example, a capsule endoscopy offers a painless and noninvasive inspection for the entire gastrointestinal tract. However, the capsule endoscopy cannot be monitored during the diagnostic inspection [3]. Many researchers adopted magnetic tracking approach to locate the capsule endoscope inside the human body in real-time [4].

Schlageter *et al.* proposed a magnetic tracking system based on Levenberg-Marquardt (LM) optimization algorithm, which was based on a 4×4 array of 16 Hall sensors, with the mean tracking errors of 3mm and 1.2° in the test distance up to 140mm [5]. Hu *et al.* built a LM algorithm-based magnetic tracking system for wireless capsule, which

The associate editor coordinating the review of this manuscript and approving it for publication was Mohammad Anwar Hossain.

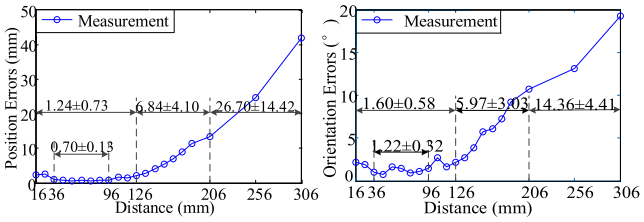

FIGURE 1. Relationship between tracking errors and the distance from magnetometer array to magnet [2]. During the experiment, a permanent magnet was tracked when it was placed above the magnetometer array. Employed magnetometers were LSM303D from STMicroelectronics Inc., Switzerland.

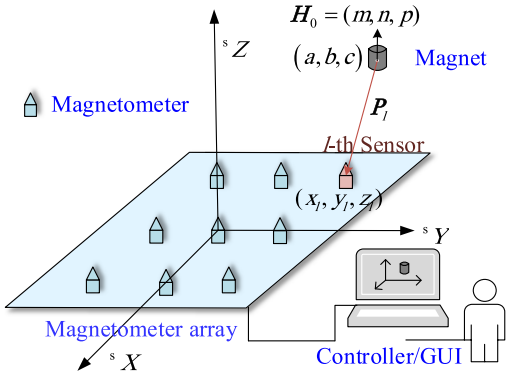

FIGURE 2. System composition of the magnetic tracking system, which refers to the magnetometer array frame {S}. H_0 = (m, n, p) is the orientation vector of the permanent magnet, with the constraint $m^2 + n^2 + p^2 = 1$. The position of the l-th sensor is (x_l, y_l, z_l). P_l represents the position vector from the magnet center (a, b, c) to the l-th sensor (x_l, y_l, z_l). GUI denotes the graphical user interface.

embedded a permanent magnet [1], [8]. A cubic sensor array, consisted of 64 analog tri-axial Anisotropic Magneto Resistance (AMR) sensors (HMC1043, Honeywell Inc., USA), was employed to track the magnet in the space of $1m^3$, with the mean tracking accuracy of 1.8mm and 1.54° [1]. Son *et al*. developed a magnetic localization setup for an untethered mesoscale magnetic robot [29]. The resulting position error was 2.1mm, and the orientation error was 6.7° within the applicable range of 50mm. Sherman *et al*. developed a system using a planar array of 27 magnetic sensors [32]. The position and orientation of a magnet (Ø4.55 × 6.35mm, remanence Br = 1.31±0.01T) were determined, while maximum errors were 3.8mm and 4.2° respectively. Song *et al*. [33] presented a magnetometer layout strategy and built a magnetic tracking system based on the layout optimization results of the entire domain. The average position and orientation error were 1.4mm and 3.4° respectively. Su *et al*. built a magnetic tracking system based on the Particle Swarm Optimization - Levenberg-Marquardt (PSO-LM) algorithm to track the single permanent magnet [2]. The most effective tracking distance ranged from 36mm to 96mm, with mean position and orientation error of 0.70mm and 1.22° respectively. However, most of these researches only presented the mean accuracy at a certain distance from the magnet to the magnetometer array. As shown in Fig. 1, the accuracy-versus-distance relationships via experiments were investigated in our previous study [2], [6]. We concluded that the tracking error rapidly increased along the distance when it was more than 106mm. The tracking error was more than 40mm at a distance of 306mm.

However, low tracking error and further tracking range are needed for most situations. Therefore, the tracking range should be improved when magnetic tracking systems are utilized widely.

Two novelties are helpful to extend the tracking distance in this study. On the one hand, state-of-the-art magnetometers with more excellent performance were adopted. On the other hand, a fusion approach with a novel tracking algorithm was proposed.

The rest of this paper is arranged as follows. Section II proposes the magnetic tracking system and task description. Section III describes the implementation of magnetic tracking algorithms. Section IV presents the prototype implementation of the tunneling magnetoresistance (TMR) -based magnetic tracking system. Experiments are demonstrated in Section V, followed by the conclusions in Section VI.

II. MAGNETIC TRACKING SYSTEM AND TASK DESCRIPTION

A. DIPOLE MODEL AND SYSTEM COMPOSITION

A cylindrical permanent magnet was adopted in this study. The magnetic field intensity of the magnet can be represented by a tri-axial magnetic dipole source [1], although there is inconsistent between the dipole model and the real spatial magnetic field distribution [27]. Based on the sensor data of more than two tri-axial magnetometers, which were in fixed positions and stationary state to sense the distribution of the magnet's magnetic field intensity, the position and orientation of the magnet can be estimated.

The magnetic tracking system composition is shown in Fig.2. The magnet pose refers to the coordinate frame of the magnetometer array frame $\{S\}$, where (a, b, c) and (m, n, p) are the position and orientation of the magnet respectively.

The tri-axial magnetic field intensity vector $\boldsymbol{B_l}$at the l-th sensor (x_l, y_l, z_l) can be formulated as follows:

$$\mathbf{B}_l = B_{lx}\mathbf{i} + B_{ly}\mathbf{j} + B_{lz}\mathbf{k} = B_T\left(\frac{3(\mathbf{H}_0 \cdot \mathbf{P}_l)\mathbf{P}_l}{|\mathbf{P}_l|^5} - \frac{\mathbf{H}_0}{|\mathbf{P}_l|^3}\right) \quad (l = 1, 2, \ldots, M), \tag{1}$$

where B_T is a constant related to the magnetic intensity of the magnet; M is the number of the magnetometers. The unit coordinate vectors were denoted as $\boldsymbol{i}, \boldsymbol{j}$, and $\boldsymbol{k}$ corresponding to the axes x, y, and z respectively.

According to (1), the magnetic field strength of the magnetic dipole decreases dramatically along with the distance from the dipole centre [2]. The magnetic field intensity around the permanent magnet is exceedingly large, whereas the magnetic field intensity in the distance of more than 300mm is small. Thus, the adopted magnetometers play a crucial role in the performance of the magnetic tracking approach.

TABLE 1. Comparative specifications of magneto resistive sensors.

Sensing Type	Hall-Effect	AMR	GMR	TMR
Power Consumption(mA)	5-20	1-10	1-10	0.001-0.01
Sensitivity (mV/V/mT)	0.005	0.1	0.3	10
Dynamic Range (mT)	1000	1	10	100
Resolution (nT/$\sqrt{Hz}$)	>100	0.1-10	1-10	0.1-10

B. MAGNETIC SENSING TECHNOLOGIES

There are a series of magnetic sensing techniques. Induction coils are with unlimited sensing range, but with big dimensions [7]. Fluxgates are suitable for low field application, but their dimensions are too large [8]. Superconducting quantum interference device (SQUID) sensors are useful for ultra-low field application but are limited to the low-temperature condition [9]. Hence, they are not suitable for the magnetic tracking approach.

Until now, there are four major generations of magnetoresistive sensors: Hall effect sensors, AMR sensors, giant magnetoresistance (GMR) sensors, and TMR sensors [10].

At first, the Hall effect sensors were utilized, such as in [5]. The main drawbacks of this sensor are their high-power consumption and low sensitivity. At present, most magnetic tracking systems are based on AMR sensors, such as in [1], [2]. However, the performance of AMR sensors is affected by their remanence effect, which should be removed by the set/reset action. GMR sensors possess higher sensitivity and more significant sensing range [11]. As Table I shows, the latest TMR sensors own predominant advantages over the other three types [12].

Besides, TMR sensors possess excellent recovery capability after saturation when it is close to the magnet [13].

According to Table I, TMR sensors can improve the performance of the magnetic tracking approach. Thus, we implemented the magnetic tracking system based on tri-axial TMR sensors in this study.

C. MAGNETIC DIPOLE-BASED MAGNETIC TRACKING ALGORITHMS

An error function for calculating the difference between the sensed magnetic signals and theoretical values from all magnetometers is expressed as:

$$E = \sum_{l=1}^{M} \|\mathbf{B}_{sl} - \mathbf{B}_l\|^2, \tag{2}$$

where $\mathbf{B}_{sl} = (B_{slx}, B_{sly}, B_{slz})$ is the sensed magnetic signal of the l-th magnetometer; $\mathbf{B}_l = (B_{lx}, B_{ly}, B_{lz})$ is the theoretical value based on the magnetic dipole model.

Hence, we can estimate the magnet pose by minimizing E with a constraint:

$$\begin{cases} \min & E \\ s.t. & m^2 + n^2 + p^2 = 1. \end{cases} \tag{3}$$

Thus, the optimization problem of the position and orientation of the magnet centre (a, b, c, m, n, p) is formulated as:

$$\mathbf{B}_{sl} = B_T \cdot f(a, b, c, m, n, p, x_l, y_l, z_l), \tag{4}$$

where l ranges from 1 to M; the$l$-th sensor's position (x_l, y_l, z_l) is fixed and defined before the initial tracking process; the magnet pose (a, b, c, m, n, p) are variable values.

Since the magnetic dipole model is a high-order nonlinear equation, nonlinear optimization algorithms are applied to solve the magnetic dipole model-based function, *i.e.*, (3). The nonlinear optimization algorithms, whose result is the optimal solution based on the minimization of E, possess high accuracy and fast execution speed. Newton method, Gauss-Newton method, quasi-Newton method, conjugate gradient method, and LM method [25] are typical nonlinear optimization algorithms. However, their performance is significantly affected by initial values [14]. As a heuristic search algorithm, PSO is fast and does not require initial values, but there are singular solutions, and the accuracy is greatly affected by noise [15]. To make full use of their respective advantages to achieve high speed and high accuracy, we adopted the PSO-LM algorithm.

In the near-source zone, the magnetic dipole model could achieve better performance [2]. However, the main reasons for the degradation of magnetic dipole model in the far-source zone are the biased environmental noise interference, model errors, the magnetic unevenness of the actual magnet, and magnetometer measurement errors [2], [4]. As a typical soft computing method, which does not require an accurate model, artificial neural networks (ANN) have been widely used for nonlinear optimization problems. It also can approximate any function with excellent accuracy due to its outstanding fault tolerance, self-organization, and exceptional learning capability [16], [18]. Thus, ANN was adopted in this study.

The ANN model, trained through experimental data, integrated the installation errors, model errors, and the inherent characteristics of the adopted magnetometers. As one of the most widely applied ANN models, the Back Propagation Neural Network (BPNN) method can provide a reasonable nonlinear approximation [17]. The BPNN model contains the following advantages: 1) allowing large errors in the samples or even individual wrong samples; 2) BPNN is the global approximation of a nonlinear mapping. In addition, BPNN based on prior knowledge should be employed because it is difficult to collect training samples. The prior knowledge can be transformed into constraints to optimize the traditional neural networks to improve generalization ability. Therefore, this study proposed the prior knowledge-based back propagation neural network (PKBPNN) method to estimate the nonlinear relation between the magnetometer outputs and magnet pose parameters.

To retain the advantages of the two algorithms at different zones, an adaptive fusion approach of the PSO-LM and PKBPNN based on the sigmoid method was proposed.

III. IMPLEMENTATION OF TRACKING ALGORITHMS

A. TRACKING ALGORITHM FOR THE NEAR-SOURCE ZONE

LM algorithm was adopted in consideration of real-time, accuracy, and excellent local search ability. However, the LM algorithm requires an initial value during the iterative process. If the initial value is not given an appropriate value, the algorithm will fall into the local optimum. PSO algorithm has the characteristics of a random sprinkling, which approximates the optimal value from the global, and does not need to set the initial value [20]. The fitness function of PSO algorithm is the total error E defined by (2). In this study, solution dimension was 5. The g-th particle was $\boldsymbol{q}_g = (q_{g1}, q_{g2}, q_{g3}, q_{g4}, q_{g5})$ $(1 \leq g \leq P)$, where P is the total number of particles and was set to 100 in this study. First, the particle's position and velocity are initialized, and the fitness value of each particle is calculated correspondingly. Then the individual extremum and the global extremum are updated according to the principle that the fitness value is as small as possible. Then the position and speed of the particles are updated according to the PSO update rules [23], [24]. If the end condition is satisfied (the error is small enough, or the maximum number of loops is reached), then program exits. Otherwise, the loop would be repeated [2]. Finally, the output value of the program is the global extremum.

The implementation of the PSO-LM methodis as follows:

1) The PSO algorithm is repeatedly performed for three times to search the solutions independently;

2) The optimum global extremum with minimum fitness function is used as the initial estimate of LM algorithm;

3) Calculating the magnet pose using the LM method;

4) In the subsequent tracking process, the results of the previous LM algorithm are taken as the initial guess value of the next calculation of the LM algorithm. The next calculation results are used as new position and orientation of magnets.

Thus, the error expression based on the magnetic dipole, *i.e.*, (3) is calculated using the PSO-LM algorithm, which can effectively avoid falling into local extremum.

B. TRACKING ALGORITHM FOR THE FAR-SOURCE ZONE

A three-layer BPNN can approximate any smooth nonlinear function with arbitrary precision [21]. However, there is an over-fitting problem because of the complex BPNN structure. To avoid the over-fitting problem and enhance the generalization ability of the network model, we propose a PKBPNN model as shown in Fig. 3.

To train the PKBPNN, the magnet should be placed evenly in the whole tracking domain. The 27-channel sampled data of the nine tri-axial magnetometers are filtered and then adopted as the input data of the network model. The network model output is the magnet pose, *i.e.*, position (a, b, c) and orientation (m, n, p).

The sampled data $\left\{\left(X^t, Y^t\right) | t = 1, 2, 3, \ldots, N\right\}$ is defined as train dataset, where $N$is the number of training samples. $X^t = \left[x_1^t, x_2^t, x_3^t, \ldots, x_{27}^t\right]^T$is the input vector, and $Y^t = \left[y_1^t, y_2^t, y_3^t, \ldots, y_6^t\right]^T$ is the expected output vector. t denotes the t-th sample.

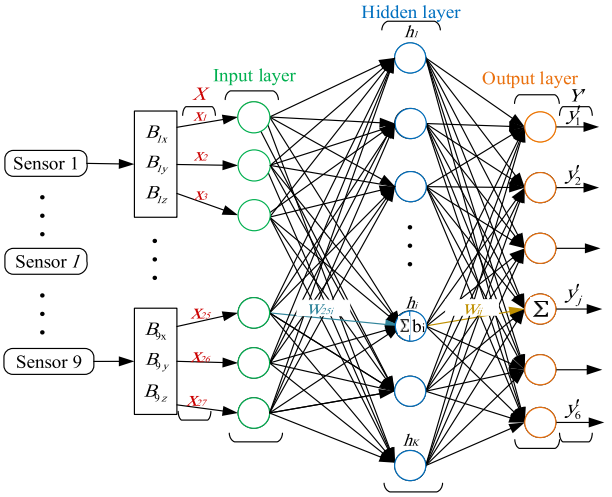

FIGURE 3. Signal flows of the PKBPNN algorithm model. There were nine tri-axial magnetometers. Hence, there were 27 PKBPNN inputs. The PKBPNN outputs were the magnet pose (*a, b, c, m, n, p*). The loss function and then network weights were optimized by using the prior knowledge of the magnetic tracking system.

The PKBPNN model, with K nodes in the hidden layer, is defined as follows:

$$\sum_{i=1}^{K} V_i f\left(W_i X^t - b_i\right) = Y^t \quad t = 1, 2, 3, \ldots, N, \tag{5}$$

where $W_i = [w_{1i}, w_{2i}, w_{3i}, \ldots, w_{27i}]$ is the weight vector connecting input nodes to the i-th hidden node; $V_i = [v_{i1}, v_{i2}, v_{i3}, \ldots, v_{i6}]^T$ is the weight vector connecting the i-th hidden nodes to output nodes; b_i is the bias of the i-th hidden node.

The transition function of the hidden layer, *i.e.*, $f(\mathrm{x})$, is the unipolar sigmoid function:

$$f(x) = 1/(1 + e^{-x}). \tag{6}$$

For the training of PKBPNN, the weights of each layer are continually adjusted through the gradient descent algorithm.

The loss function of the general network model is defined as the mean square error:

$$E_n = \frac{1}{2}\sum_{t=1}^{N}\left(e^t\right)^2 = \frac{1}{2}\sum_{t=1}^{N}\left[Y'^t - Y^t\right]^2, \tag{7}$$

where $\mathbf{Y}'^t$ is the actual output of the network; $\mathbf{Y}^t$ indicates the expected value of the target output $(a, b, c, m, n, p)^T$; e^t is the difference between the expected output and the actual output.

We add the constraint into the loss function to optimize the neural network training [28]. As the tracking domain is defined to $L_d \times W_d \times H_d$ mm^3 above the magnetometer array, boundary conditions, which functions as prior knowledge, can be added into the loss function:

$$\begin{cases} \min & E_D = \frac{1}{2}\sum_{t=1}^{N}\left[Y'^t - Y^t\right]^2 \\ s.t. & \left|Y'^t_1\right| < \frac{L_d}{2} \\ & \left|Y'^t_2\right| < \frac{W_d}{2} \\ & 0 < Y'^t_3 < H_d, \end{cases} \tag{8}$$

where Y'^t_1, Y'^t_2, Y'^t_3 represent the first, second, and third components of the t-th actual output vector, respectively, *i.e.*, y'^t_1, y'^t_2, y'^t_3 (the X-, Y-, Z- positions of the magnet).

With the advantage of the penalty function method, we can acquire the optimal solution of the constrained-optimization problem showed in (8) by constructing the following penalty function:

$$\begin{aligned} E_p = &\frac{1}{2}\sigma_1 \sum_{t=1}^{N}\left[\max\left(\left|Y'^t_1\right|, \frac{L_d}{2}\right) - \frac{L_d}{2}\right]^2 \\ &+\frac{1}{2}\sigma_2 \sum_{t=1}^{N}\left[\max\left(\left|Y'^t_2\right|, \frac{W_d}{2}\right) - \frac{W_d}{2}\right]^2 \\ &+\frac{1}{2}\sigma_3 \sum_{t=1}^{N}\left[\max\left(\left|Y'^t_3 - \frac{H_d}{2}\right|, \frac{H_d}{2}\right) - \frac{H_d}{2}\right]^2, \end{aligned} \tag{9}$$

where σ_1, σ_2, and σ_3 are penalty factors of the penalty function.

The loss function with prior knowledge, *i.e.*, (9), can be described as follows:

$$\begin{aligned} \min E_D = &\sum_{t=1}^{N}\left\{\frac{1}{2}\left[Y'^t - Y^t\right]^2\right. \\ &+\frac{1}{2}\sigma_1\left[\max\left(\left|Y'^t_1\right|, \frac{L_d}{2}\right) - \frac{L_d}{2}\right]^2 \\ &+\frac{1}{2}\sigma_2\left[\max\left(\left|Y'^t_2\right|, \frac{W_d}{2}\right) - \frac{W_d}{2}\right]^2 \\ &\left.+\frac{1}{2}\sigma_3\left[\max\left(\left|Y'^t_3 - \frac{H_d}{2}\right|, \frac{H_d}{2}\right) - \frac{H_d}{2}\right]^2\right\} \\ = &\min\left\{E_n + E_p\right\} \end{aligned} \tag{10}$$

.

This training process is stopped when the predefined error of the PKBPNN output or the preset iterated time of training is satisfied. Finally, the PKBPNN's parameters can be derived.

C. FUSION STRATEGY

The distance-dependent fusion strategy for a more considerable tracking distance is presented in Fig. 4. The PSO-LM algorithm is performed when the tracking distance ranged from 0 to D_1. For the tracking distance ranged from D_2 to D_3, the PKBPNN algorithm is adopted. For the tracking distance ranged from D_1 to D_2, *i.e.*, the transition zone, its extent can be regulated according to the actual condition.

When the tracking range is bigger than D_3, the magnetic tracking system is invalid, which means the tracking accuracy could not meet most application requirements [19].

The magnet pose in the transition zone can be described as follows:

$$\begin{cases} [a_t, b_t, c_t, m_t, n_t, p_t] = \lambda\,[a_n, b_n, c_n, m_n, n_n, p_n] \\ \qquad\qquad +(1-\lambda)[a_f, b_f, c_f, m_f, n_f, p_f] \\ \dfrac{1}{\lambda} = 1 + e^{\left(-\frac{(c_f - (D_2+D_1)/2)*s}{(D_2-D_1)/2}\right)}, \end{cases} \tag{11}$$

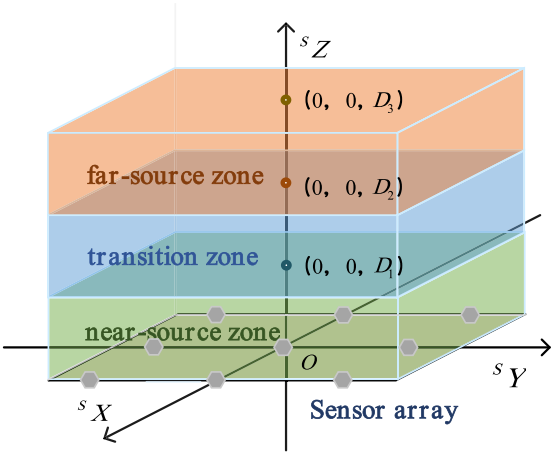

FIGURE 4. Diagram plot of fusion strategy between the distance and tracking algorithms. Here D_1, D_2, and D_3 in Z-axis represent the distance from the magnetometer array to the permanent magnet. The unit of D_1, D_2, *and* D_3 is mm.

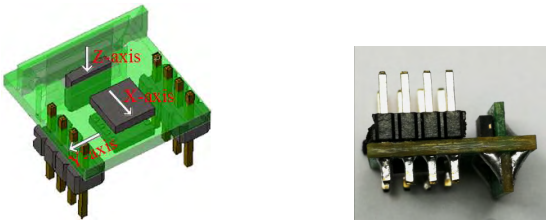

FIGURE 5. System diagram (Left) and physical map (Right) of the TMR2305, with full scale at ±400uT and resolution at 0.016uT. The distance from Z-axis to Y-axis was 4.9mm; the distance from the X-axis to the Y-axis was 1.75mm.

where D_1, D_2, and D_3 are determined by the experimental results of the magnetic tracking system; $[a_n, b_n, c_n, m_n, n_n, p_n]$ is the magnet position and orientation calculated by PSO-LM algorithm; $[a_t, b_t, c_t, m_t, n_t, p_t]$ is the magnet position and orientation of the transition zone; $[a_f, b_f, c_f, m_f, n_f, p_f]$ is the magnet position and orientation calculated by the PKBPNN algorithm; λ is the fusion coefficient; s is the speed factor and represents the speed of the transition, *i.e.*, large value represents the fast transition.

IV. PROTOTYPE IMPLEMENTATIONS

In this study, we implemented the prototype of the TMR-based magnetic tracking system.

To compare the TMR-based system with the AMR-based system, the dimension of the planar magnetometer array and the magnetometer number were the same as those of our previous studies [2], [6]. The array size is 150 × 150mm^2, and the magnetometer number is 9.

A. TMR SENSOR ARRAY-BASED MAGNETIC TRACKING PROTOTYPE

TMR emerged firstly for the magnetic disc application, which only needs a single axis sensing. To carry out magnet pose tracking, tri-axial magnetometers (TMR2305, Doways Inc., China) were adopted. Fig. 5 shows the system diagram and physical map of the TMR2305.

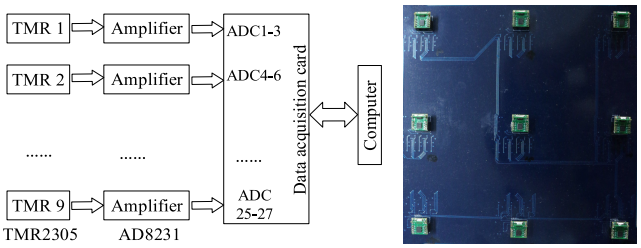

FIGURE 6. Left: System diagram of the TMR-based magnetic tracking system. Right: Prototype of the magnetometer array.

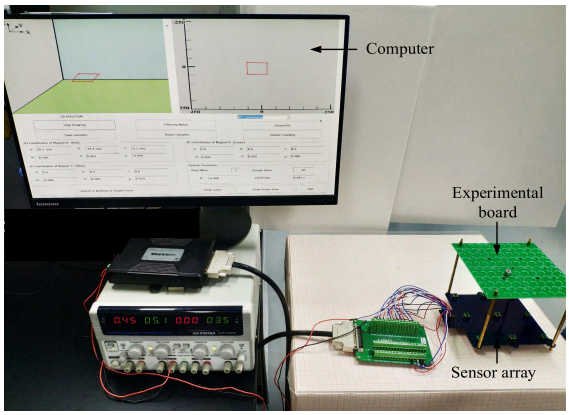

FIGURE 7. Experimental platform for the TMR-based magnetic tracking system. The distance from the sensor array to the experimental board was 76mm in this figure.

Fig. 6 shows the system diagram of the TMR-based magnetic tracking system. As TMR sensors are with analog output, amplifiers with adjustable amplitude were adopted to amplify the TMR sensors signals. The amplifier outputs were connected to the Data Acquisition Card (DAQ Card), and the amplitude of each amplifier was controlled via the output pins of the DAQ Card. The digital sensor data were then transmitted to the computer for further signal processing and algorithm implementation. The magnetometers and amplifiers were welded on a single printed circuit board.

B. MAGNETOMETER CALIBRATIONS

There were types of errors for magnetometer measurements. One was the errors resulted from the manufacturing processes, and the other was the external influences that resulted from the environment magnetics and geomagnetic vectors. These two types of errors should be removed or counteracted by magnetometer calibration procedures.

Calibration procedures for both AMR and TMR sensors were the same, include calibrations of the bias, scaling factor, and cross-axis misalignment [22].

V. EXPERIMENTS

A. EXPERIMENTAL PLATFORM AND PROCEDURES

In this study, we used an axially magnetized cylindrical N35 Nd-Fe-B magnet (Ø10mm × 10mm, $B_T = 8.1 \times 10^{-8}$T, remanence $Br = 1.22 \pm 0.01$T) as the magnetic source. The tracking domain was defined to $150 \times 150 \times 400$mm^3 above the magnetometer array

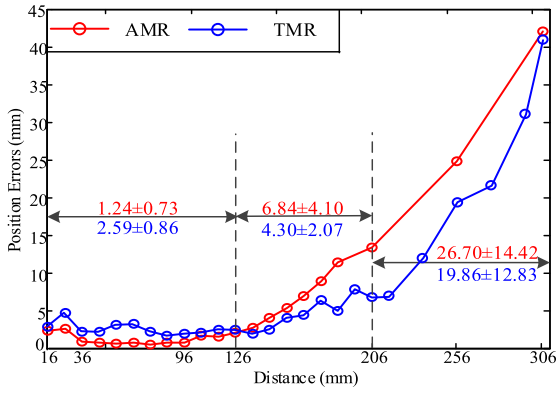

FIGURE 8. Relationships between position errors and tracking distance. The red line denotes the data from the AMR-based tracking prototype in our previous study [2]. The blue line represents the data from the TMR-based tracking prototype in this study.

Fig. 7 shows the experimental platform. To precisely locate the magnet, an experimental board was designed and placed on the upper side of the magnetometer array. The experimental board was inscribed with scales and evenly carved 111 holes to locate the magnet. The distance from the magnetometer array to the experimental board can be adjusted via adjustable support legs.

The setting and operations of the magnetic tracking prototypes were carried out in the host computer's graphical user interface (GUI), which was developed based on VS2010 (Microsoft Inc., USA).

To evaluate the tracking performance, the measurements of the prototype were carried out with the same tracking conditions as the previous study [2].

B. COMPARISON OF TRACKING PERFORMANCE OF PSO-LM ALGORITHM BETWEEN AMR AND TMR SENSORS

At first, the PSO-LM algorithm was performed with the tracking distance from 16mm to 306mm. During the experiment, we measured 25 points evenly in the experiment board for each defined tracking distance, *i.e.*, the distance from the magnet to the magnetometer array. The measurement interval from 16mm to 216mm was 10mm, and the measurement interval from 216mm to 306mm was 20mm.

Based on TMR sensor array and AMR sensor array, the relationships betweent tracking errors and tracking distance were shown in Fig. 8 and Fig. 9.

The TMR-based prototype had the most exceptional performance when the tracking distance ranged from 16mm to 166mm, where the average position and orientation errors were 2.73 ± 0.92mm and $3.24 \pm 1.15°$ respectively. When the tracking distance was bigger than 166mm, the tracking errors increased with the increase of tracking distance. For the tracking distance ranged from 176mm to 236mm, the average position and orientation errors were 7.45 ± 2.41mm and $8.95 \pm 0.60°$ respectively. The mean position and orientation errors were 28.37 ± 9.90mm and $16.10 \pm 4.45°$ respectively when the tracking distance ranged from 256mm to 296mm. The mean position error and mean orientation error

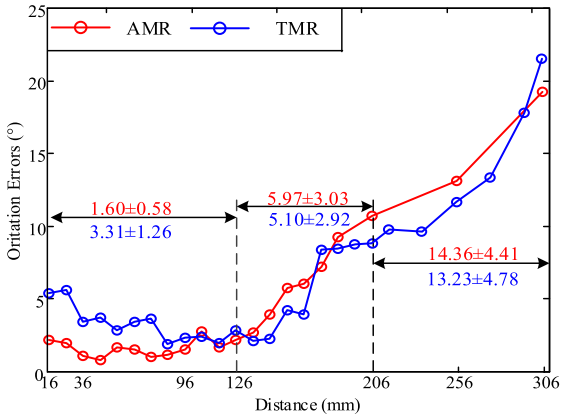

FIGURE 9. Relationships between orientation errors and tracking distance. The red line denotes the data from the AMR-based tracking prototype in our previous study [2]. The blue line represents the data from the TMR-based tracking prototype in this study.

were 41.1mm and 21.53° respectively when the tracking distance was 306mm. When the tracking distance was exceeded 306mm, the positioning errors of PSO-LM method were more than 40 mm.

In order to maintain the tracking accuracy of near-source zone as much as possible, we defined the D_1 as 216mm.

According to Fig. 8 and Fig. 9, the AMR-based prototype had superior tracking performance for tracking distances less than 126mm, whereas the TMR-based prototype had superior performance when tracking distance was bigger than 136mm.

The reason was supposed that the physical dimension of TMR2305 was much bigger than AMR, *i.e.*, LSM303D in [2]. Their physical dimensions were $9.5 \times 9.5 \times 6\text{mm}^3$ and $5 \times 5 \times 0.79\text{mm}^3$ respectively. At the same time, dimensions of the magnet were Ø10mm × 10mm. According to the definition of magnetic dipole model [7], a restriction was that the distance from the test field point, *i.e.*, the magnetometer position, to the magnet should be large enough compared with the magnet size. Otherwise, the near-field problem resulted in inaccurate dipole model [26].

C. EVALUATION OF FUSION STRATEGY BASED ON TMR SENSORS

In the neural network modeling, the number of nodes in the input layer was chosen as 27 since nine tri-axial magnetometers were adopted. The number of nodes in the output layer was selected as six since the 6D magnet pose was needed. The number of hidden layer nodes was chosen as 20. The number of hidden layer nodes was determined experimentally to have enough approximation ability without increasing the complexity. To make the trained model powerfully transplantable, the ambient magnetic field needed to be measured and recorded at the beginning of collecting data. The initial magnetic field was removed from the collected data.

The evaluation of PKBPNN was carried out as following steps.

Firstly, 1110 points, *i.e.*, 111 points of each tracking distance (206mm, 226mm, 246mm, 266mm, 286mm, 306mm,

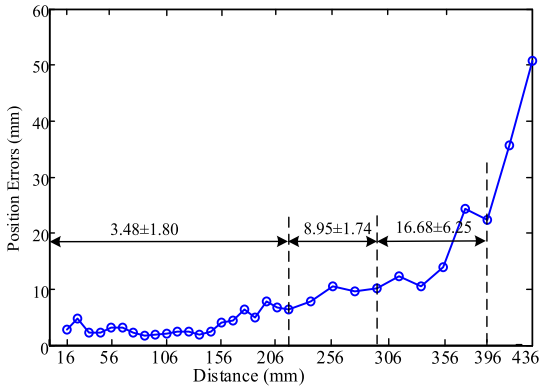

FIGURE 10. Plot of the position errors versus the distance between the magnetometer array and the magnet.

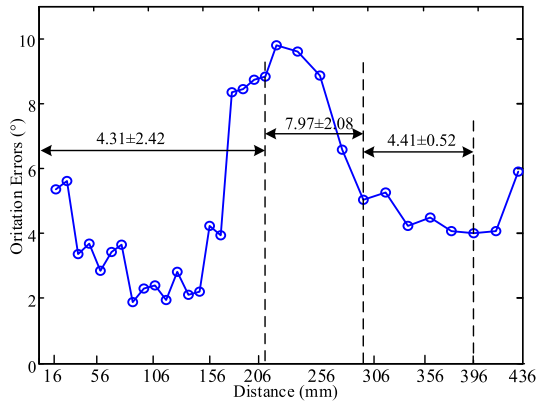

FIGURE 11. Plot of the orientation errors versus the distance between the magnetometer array and the magnet.

326mm, 346mm, 366mm, 386mm), were sampled for the implementation of PKBPNN's model. Each point was repeatedly measured ten times, whose mean value was defined as the PKBPNN's data. The implementation of PKBPNN model was arranged as follows:

1) The random 70% of the neural network's total data set, *i.e.*, 776 points, were adopted as the training data set.
2) Then other random 15% of the neural network's total data set, *i.e.*, 167 points, were adopted to validate the PKBPNN model to adjust itself parameters.
3) The remaining 15% of the neural network's total data set, *i.e.*, 167 points, were adopted to test the PKBPNN model.

In the experiment, the learning rate η was 0.6, the expected error was 0.001, and the penalty factor vector (σ_1, σ_2, σ_3) was (0.046, 0.045, 0.051). Besides, the maximum number of iterations was 1000.

In the second step, the real-time magnet pose is tracking via the trained PKBPNN model. The PKBPNN model was evaluated on the tracking distances (216mm, 236mm, 256mm, 276mm, 296mm, 316mm, 336mm, 356mm, 376mm, 396mm, 416mm, 436mm). Five points in the experimental board were measured for each tracking distance, and each point was repeatedly measured five times.

Magnetic tracking performance for the tracking distance from 16mm to 436mm was showed in Fig. 10 and Fig. 11.

TABLE 2. Statistic analysis of the tracking errors base on TMR sensors.

Distance (mm)		0 - D_1	D_1 - D_2	D_2 - D_3
PSO-LM	E_p (mm)	3.48±1.80	18.24±9.37	41.10
	E_o (°)	4.31±2.42	12.45±3.37	21.53
Proposed method	E_p (mm)	3.48±1.80	8.95±1.74	16.68±6.25
	E_o (°)	4.31±2.42	7.97±2.08	4.41±0.52

E_p denotes position error; E_o represents orientation error. Tracking errors in this table were root-mean-square (RMS) values. Values marked with red denote the PKBPNN-based tracking results. For the PSO-LM based tracking results between D_2 and D_3 mm, only the tracking point 306mm was measured as the tracking errors increased rapidly and were not stable.

It can be found from Fig. 8–11, the tracking performance for the tracking distance ranged from 256mm to 396mm had significantly improved. The position errors and orientation errors were 14.74 ± 6.08mm and 4.81 ± 0.92° respectively when the tracking distance ranged from 256mm to 396mm. As the magnetic signal decreased rapidly along with the tracking distance, D_2 and D_3 were defined as 296mm and 396mm according to the PKBPNN tracking performance. When the distance was bigger than 396mm, PKBPNN methods cannot effectively locate the magnetic posture.

E_p denotes position error; E_o represents orientation error. Tracking errors in this table were root-mean-square (RMS) values. Values marked with red denote the PKBPNN-based tracking results. For the PSO-LM based tracking results between D_2 and D_3 mm, only the tracking point 306mm was measured as the tracking errors increased rapidly and were not stable.

The tracking performance comparison between the proposed fusion method and PSO-LM method was shown in Table II based on the TMR sensors. It can be found from Table II, and the pose tracking errors were reduced from (18.24 ± 9.37mm, 12.45 ± 3.37°) to (8.95 ± 1.74mm, 7.97±2.08°) for the tracking range between 216mm and 296mm. Position error and orientation error were reduced by 50.93% and 35.98%, respectively. Also, tracking distances were extended to 396 mm, with the position error (16.68 ± 6.25mm) and orientation error (4.41 ± 0.52°). However, the position error and orientation error of PSO-LM algorithm were 41.10mm and 1.2° respectively when the distance was 306 mm. It can be concluded that the fusion approach with TMR-based magnetic tracking system has significantly extended the tracking range of the magnetic tracking system.

D. DISCUSSION

PSO-LM had more exceptional tracking performance when the magnet was close to the magnetometer array. With its prominent nonlinear mapping ability and fault tolerance, the PKBPNN algorithm possessed excellent tracking performance when the tracking distance was bigger than the valid PSO-LM tracking domain. Considering the overall tracking domain, a fusion strategy based on PSO-LM and PKBPNN was proposed. The boundaries between the near-source zone and the far-source zone were set as the transition zone, where the two algorithms were fused.

The PSO-LM tracking performance, by comparison of AMR-based and TMR-based tracking prototypes, was showed in Fig. 8 and Fig. 9. For the PSO-LM and TMR-based magnetic tracking method, the tracking errors were raised sharply along with the tracking distance since D_1, *i.e.*, 216 mm. For tracking distance less than 126mm, AMR-based position errors were smaller than that of the TMR-based prototype. The reason may be that AMR sensors possess the advantages of mature technology and stable performance, whereas TMR sensors are currently with unstable quality.

At present, tri-axial TMR sensors are expensive (>$100 per sensor) and only available in Doways Inc. [12]. We chose TMR2305, which had the worst parameters in their tri-axial TMR sensor series and were easy to damage, for economic consideration. For tracking distance above 126mm, TMR-based prototypes achieved better tracking performance. The reason is that the TMR sensors possess higher sensitivity than that of AMR sensors.

To extend the tracking range, we proposed a novel fusion strategy. According to different tracking distances, PSO-LM and PKBPNN are fused with different weights in the transition region.

More exceptional approximation ability and generalization ability were achieved by using the prior knowledge of the magnetic tracking system to optimize the loss function and the network weights.

The comparison between PSO-LM and the fusion strategy in the tracking domain (16mm, 396mm) is shown in Table II. The tracking range and accuracy were significantly improved by using this method we proposed during the tracking domain (216mm, 396mm). Experimental results showed that the tracking errors decreased sharply from (18.24 ± 9.37mm, 12.45 ± 3.37°) to (8.95 ± 1.74mm, 7.97 ± 2.08°) within the distance range of 216mm to 296mm.

LM was employed by most of the related studies [1], [5], [29], [30], [31], without the help of the ANN algorithm. However, their application prospects were limited by the short effective tracking distance. For example, Son *et al.* [29] achieved the pose accuracies of (2.1 ± 0.8mm, 6.7 ± 4.3°) between the range (5mm, 150mm), based on the 64 Hall-effect sensors array. Popek *et al.* [30] reported the pose accuracies at (11mm, 11°) at the range between 136mm and 144mm. Di Natali *et al.* [31] proposed the pose accuracies of (3.4 ± 3.2 mm, 19 ± 50°) at the range of 150mm. It could be found that the proposed tracking method possessed a more extensive tracking range with superior pose accuracy.

VI. CONCLUSION

Magnetic tracking has no line-of-sight problem. However, there is limited tracking range, which restricts its feasibility and practicability.

In this study, we developed a novel magnetic tracking prototype based on state-of-the-art tri-axial TMR sensors and PKBPNN method for tracking range extending. The prior knowledge of the magnetic tracking system, *i.e.*, the defined tracking domain in its practical applications, was utilized to

optimize the loss function and network weights of PKBPNN model. Compared with the PSO-LM algorithm, experimental results showed that the fusion approach had better tracking performance during the tracking domain (216mm∼396mm). This prototype firstly extended the tracking range to more than 356mm, when the position error was less than 15mm.

In the future work, an automatic measurement method will be used to improve the training efficiency of PKBPNN, which means a robotic can be utilized to place automatically the magnet in the whole tracking domain to obtain the training data set. Furthermore, advanced tracking algorithms, such as deep learning methods, should be investigated [9]. Besides, the tri-axial TMR sensors are still not mature, despite their overwhelming potential technical advantage over existing magnetic sensing techniques. The TMR sensor-based tracking system can be more accurate and robust along with the exciting development of smart TMR sensors. Thus, the magnetic tracking system can be widely applied in the biomedical and industrial area.

ACKNOWLEDGMENT

(Bowen Lv and Yuangui Chen contributed equally to this work.)

REFERENCES

[1] C. Hu, M. Li, S. Song, W. Yang, R. Zhang, and M. Q.-H. Meng, "A cubic 3-axis magnetic sensor array for wirelessly tracking magnet position and orientation," *IEEE Sensors J.*, vol. 10, no. 5, pp. 903–913, May 2010.

[2] S. Su *et al.*, "Investigation of the relationship between tracking accuracy and tracking distance of a novel magnetic tracking system," *IEEE Sensors J.*, vol. 17, no. 15, pp. 4928–4937, Aug. 2017.

[3] G. Iddan, G. Meron, A. Glukhovsky, and P. Swain, "Wireless capsule endoscopy," *Nature*, vol. 405, p. 417, May 2000.

[4] C. Hu, Y. Ren, X. You, and W. Yang, "Locating intra-body capsule object by three magnet sensing system," *IEEE Sensors J.*, vol. 16, no. 13, pp. 5167–5176, Jul. 2016.

[5] V. Schlageter, P.-A. Besse, R. Popovic, and P. Kucera, "Tracking system with five degrees of freedom using a 2D-array of Hall sensors and a permanent magnet," *Sens. Actuator A Phys.*, vol. 92, no. 1, pp. 37–42, Aug. 2001.

[6] H. Dai, C. Hu, S. Su, M. Lin, and S. Song, "Geomagnetic compensation for the rotating of magnetometer array during magnetic tracking," *IEEE Trans. Instrum. Meas.*, to be published.

[7] E. Paperno and A. Plotkin, "Cylindrical induction coil to accurately imitate the ideal magnetic dipole," *Sens. Actuators A, Phys.*, vol. 112, nos. 2–3, pp. 248–252, May 2004.

[8] J. Jeng, C. Lu, C. Shiue, and V. Luong, "Monolithic three-axis fluxgate magnetometer," in *Proc. Int. Conf. Asian Union Magn. Societies (ICAUMS)*, Taiwan, China, Aug. 2016, p. 1.

[9] J. E. McGary, "Real-time tumor tracking for four-dimensional computed tomography using SQUID magnetometers," *IEEE Trans. Magn.*, vol. 45, no. 9, pp. 3351–3361, Sep. 2009.

[10] H. Heidari, F. Liu, and R. Dahiya, "Towards flexible magnetoelectronics for robotic applications," in *Proc. 2nd Asia–Pacific Conf. Intell. Robot Syst. (ACIRS)*, Wuhan, China, Jun. 2017, pp. 295–298.

[11] C. Reig, M.-D. Cubells-Beltrán, and D. R. Muñoz, "Magnetic field sensors based on giant magnetoresistance (GMR) technology: Applications in electrical current sensing," *Sensors*, vol. 9, no. 10, pp. 7919–7942, Oct. 2009.

[12] MultiDimension Technology. (2018). *Introduction to TMR Magnetic Sensors*. [Online]. Available: http://www.dowaytech.com/en/1776.html

[13] X. Yuan, W. Li, G. Chen, X. Yin, and J. Ge, "Circumferential current field testing system with TMR sensor array for non-contact detection and estimation of cracks on power plant piping," *Sens. Actuators A, Phys.*, vol. 263, pp. 542–553, Aug. 2017.

[14] N. Checchi, E. Giusti, and S. Marsili-Libelli, "PEAS: A toolbox to assess the accuracy of estimated parameters in environmental models," *Environ. Model. Softw.*, vol. 22, no. 6, pp. 899–913, Jun. 2007.

[15] M. R. Bonyadi and Z. Michalewicz, "Particle swarm optimization for single objective continuous space problems: A review," *Evol. Comput.*, vol. 25, no. 1, pp. 1–54, 2016.

[16] N. P. Padhy and S. P. Simon, *Soft Computing: With MATLAB Programming*. New York, NY, USA: Oxford Univ. Press, 2015, pp. 63–282.

[17] D. E. Rumelhart, G. E. Hinton, and R. J. Williams, "Learning representations by back-propagating errors," *Nature*, vol. 323, pp. 533–536, Oct. 1986.

[18] M. Qasim and V. Khadkikar, "Application of artificial neural networks for shunt active power filter control," *IEEE Trans. Ind. Informat.*, vol. 10, no. 3, pp. 1765–1774, Aug. 2014.

[19] H. Dai, S. Song, C. Hu, B. Sun, and Z. Lin, "A novel 6-D tracking method by fusion of 5-D magnetic tracking and 3-D inertial sensing," *IEEE Sensors J.*, vol. 18, no. 23, pp. 9640–9648, Dec. 2018.

[20] J. Robinson and Y. Rahmat-Samii, "Particle swarm optimization in electromagnetics," *IEEE Trans. Antennas Propag.*, vol. 52, no. 2, pp. 397–407, Feb. 2004.

[21] H. K. Lam *et al.*, "Variable weight neural networks and their applications on material surface and epilepsy seizure phase classifications," *Neurocomputing*, vol. 149, pp. 1177–1187, Feb. 2015.

[22] T. Pylvänäinen, "Automatic and adaptive calibration of 3D field sensors," *Appl. Math. Model.*, vol. 32, no. 4, pp. 575–587, 2008.

[23] W. Yang, C. Hu, M. Q.-H. Meng, S. Song, and H. Dai, "A six-dimensional magnetic localization algorithm for a rectangular magnet objective based on a particle swarm optimizer," *IEEE Trans. Magn.*, vol. 45, no. 8, pp. 3092–3099, Aug. 2009.

[24] S. Su *et al.*, "Positioning accuracy improvement of automated guided vehicles based on a novel magnetic tracking approach," *IEEE Intell. Transp. Syst. Mag.*, to be published.

[25] C. Kanzowa, N. Yamashitab, and M. Fukushima, "Levenberg–Marquardt methods with strong local convergence properties for solving nonlinear equations with convex constraints," *J. Comput. Appl. Math.*, vol. 172, no. 2, pp. 375–397, Dec. 2004.

[26] Y. Ren, C. Hu, S, Xiang, and Z. Feng, "Magnetic dipole model in the near-field," in *Proc. IEEE Int. Conf. Inf. Automat. (ICIA)*, Aug. 2015, pp. 1085–1089.

[27] S. Nedelcu1 and J. H. P. Watson, "Magnetic dipole model of a permanent magnet based device," *J. Phys. D, Appl. Phys.*, vol. 34, no. 17, pp. 2622–2628, Aug. 2001.

[28] H. Dai, G. Zhao, M. Lin, J. Wu, and G. Zheng, "A novel estimation method for the state of health of lithium-ion battery using prior knowledge-based neural network and Markov chain," *IEEE Trans. Ind. Electron.*, to be published.

[29] D. Son, S. Yim, and M. Sitti, "A 5-D localization method for a magnetically manipulated untethered robot using a 2-D array of Hall-effect sensors," *IEEE/ASME Trans. Mechatronics*, vol. 21, no. 2, pp. 708–716, Apr. 2016.

[30] K. M. Popek, A. W. Mahoney, and J. J. Abbott, "Localization method for a magnetic capsule endoscope propelled by a rotating magnetic dipole field," in *Proc. IEEE Int. Conf. Robot. Automat.(ICRA)*, May 2013, pp. 5328–5333.

[31] C. Di Natali, M. Beccani, and P. Valdastri, "Real-time pose detection for magnetic medical devices," *IEEE Trans. Magn.*, vol. 49, no. 7, pp. 3524–3527, Jul. 2013.

[32] J. T. Sherman, J. K. Lubkert, R. S. Popovic, and M. R. DiSilvestro, "Characterization of a Novel Magnetic Tracking System," *IEEE Trans. Magn.*, vol. 43, no. 6, pp. 2725–2727, Jun. 2007.

[33] S. Song, X. Qiu, J. Wang, and M.-H. Meng, "Design and optimization strategy of sensor array layout for magnetic localization system," *IEEE Sensors J.*, vol. 17, no. 6, pp. 1849–1857, Mar. 2017.

BOWEN LV received the bachelor's degree in electronic information science and technology from Qufu Normal University, in 2017. She is currently pursuing the master's degrees in computer technology with the North University of China and also with the Quanzhou Institute of Equipment Manufacturing, Haixi Institutes, Chinese Academy of Sciences. Her research interest includes magnetic tracking.

YUANGUI CHEN received the B.S. and M.S. degrees from Fujian Medical University, China, in 2007 and 2011, respectively, where he is currently pursuing the Ph.D. degree in radiotherapy. His current research interest includes magnetic tracking technique in the precision radiotherapy for lung cancer.

HOUDE DAI received the M.S. degree from Tongji University, China, in 2009, and the Ph.D. degree from TU Muenchen, Germany, in 2014. He is currently a Professor with the Quanzhou Institute of Equipment Manufacturing, Haixi Institutes, Chinese Academy of Sciences. His current research interests include intelligent localization systems and mobile robot.

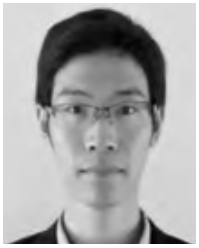

SHIJIAN SU received the B.S. and M.S. degrees in electronic science and technology from Fuzhou University, in 2012 and 2015, respectively. He is currently pursuing the Ph.D. degree with Fuzhou University. He is currently an Engineer with the Quanzhou Institute of Equipment Manufacturing, Haixi Institutes, Chinese Academy of Sciences, China. His current research interests include intelligent sensors and magnetic localization.

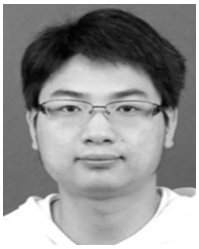

MINGQIANG LIN received the B.S. degree in automation from the University of Science and Technology of China, Hefei, China, in 2011, and the Ph.D. degree in control science and engineering from the University of Science and Technology of China, Hefei, China, in 2016. He is currently with the Quanzhou Institute of Equipment Manufacturing, Haixi Institutes, Chinese Academy of Sciences, Jinjiang, China.